DATA REPOSITORY

Methods
Figs. DR1 to DR9
Tables DR1 to DR4

METHODS

All rock magnetic and paleomagnetic measurements were made in the paleomagnetism laboratories at the University of Rochester. Magnetic hysteresis measurements were made using a Princeton Measurements Corporation Alternating Gradient Force Magnetometer, slope-correction was done by subtracting the high-field (> 70% maximum field) contribution. First order reversal curves were processed using FORCinel software (Harrison and Feinberg, 2008). Magnetic susceptibility versus temperature measurements were made using a Geofyzika KLY-4C KappaBridge. Alternating field demagnetizations were performed on standard ∼2.5 cm diameter cores, which were drilled from field oriented hand samples, using a Sapphire Instruments SI-4 Alternating Field Demagnetizer. Cores were measured using a 2G Enterprises 755 3-component DC SQUID magnetometer with high resolution sensing coils housed in a magnetically shielded room with ambient field <200 nT. Thermal demagnetization experiments on whole rocks were conducted using an ASC Model TD48-SC high-capacity single-chamber thermal specimen demagnetizer.

In assigning polarities to characteristic magnetizations isolated from feldspars (Fig. 3) we aimed at being most conservative, using the least number of assumptions. We selected the stereonet quadrant where we expected a primary shallow direction to be located on the basis of prior results (Tanczyk et al., 1987). If the shallow direction has two polarities, the reversed polarity should be located in the quadrant antipodal to the one containing the Tanczyk et al. (1987) shallow direction. Using this simple division, we isolated A and B directions and found they passed a reversal test. Directions falling outside the 2 identified quadrants were identified as transitional. These assignments were compared against an approach using virtual geomagnetic poles (see Fig. DR9); the polarity assignments were found to be consistent.

Further experiments were conducted on plagioclase crystals from Sept-Îles Layered Series anorthosites to estimate the magnetic anisotropy effects associated with the needle-like magnetic carriers. Unoriented plagioclase crystals with natural remanent magnetizations ranging from 1 to 20 x 10^{-10} A m^2 and lacking inclusions visible at 10x magnification were selected. Crystals were ∼1-3 mm in length and ∼1 mm thick. Samples were mounted on quartz rods using sodium silicate and thermally demagnetized up to 520 °C. If samples unblocked over temperature ranges equivalent to those of our directional study (i.e., ∼400-520 °C), and in orthogonal vector plots (unoriented) directions trended towards the origin, they were selected for anisotropy estimates. Samples were heated to 520 °C and allowed to cool in a 60 μT magnetizing field (imparting a total TRM), and subsequently measured. The difference between the applied (expected) field and the measured field for independent crystals is 19.9°± 4.0° (see Table DR4). Although not a full tensor calculation, we feel this value provides a useful measure of the deviation for any given paleomagnetic direction due to anisotropy (cf. Figure 3). We note that feldspars from our samples show no preferred orientation and therefore results from multiple crystals should average any anisotropy effects.

Polished 30 μm standard thin sections and epoxy-mounted isolated feldspar grains were analyzed using a Zeiss-Auriga Scanning Electron Microscope at the University of Rochester. Electron microprobe analysis (EMPA) was conducted at Cornell University using a JEOL 8900 Electron Microprobe Microanalyzer. Scanning electron microscopy was conducted under high-vacuum on polished, carbon coated samples with accelerating voltages ranging from 5–20 kV. EMPA was conducted under high-vacuum on polished, carbon coated samples at an accelerating voltage of 15 kV. EMPA standard for Iron: magnetite "Asti" Brazil; Aluminum: garnet NMH 87375; Titanium: ilmenite NMH 96189; Magnesium: garnet NMH 87375.

REFERENCES CITED

Harrison, R.J., and Feinberg, J.M., 2008, FORCinel: An improved algorithm for calculating first-order reversal curve distributions using locally weighted regression smoothing: Geochemistry, Geophysics, Geosystems, v. 9, p. Q05016, doi: 10.1029/2008GC001987.

DATA REPOSITORY FIGURES

Fig. DR1. Simplified geologic map (Higgins, 2005; Namur et al., 2010) of the Sept-Îles Intrusive Suite (SIIS). Labeled stars define sites: SI-1, 50^o 17.6′ N, 66^o 26.1′ W; SI-2, 50^o 9.3′ N, 66^o 29.8′ W; SI-3, 50^o 9.3′ N, 66^o 29.8′ W.

Fig. DR2. Whole rock magnetic hysteresis. Additional examples of magnetic hysteresis curves measured on whole rocks of SIIS layered series anorthosites.

Fig. DR3. Single silicate crystal magnetic hysteresis. Additional examples of magnetic hysteresis curves measured on single feldspars lacking visible inclusions (at ∼10x magnification) from SIIS layered series anorthosites. Inset shows non-slope corrected curves.

Fig. DR4. First order reversal curve distributions from SIIS. A: First order reversal curve distribution (FORC) measured on whole rock sample of layer series anorthosite. VARIFORC smoothing factor settings are: vertical ridge (Sc0), 14; central ridge (Sb0), 14; horizontal smoothing (Sc1), 15; vertical smoothing (Sb1), 15; and rate of increase in smoothing factor (λ), 0.1. B: FORC measured on optically clear feldspar separated from layered series anorthosite. VARIFORC smoothing factor settings are: vertical ridge (Sc0), 7; central ridge (Sb0), 7; horizontal smoothing (Sc1), 8; vertical smoothing (Sb1), 8; and rate of increase in smoothing factor (λ), 0.1.

Fig. DR5. Alternating field and thermal demagnetization of SIIS whole rocks. Boxes, inclination; circles, declination. A: Orthogonal vector plot of stepwise alternating field demagnetization of whole rock layered series anorthosite. NRM intensity is 5.19 x 10^{-6} A m^2. Inset: equal area stereonet projection, labeled points are steps in mT. Filled circles, positive inclination; open circles, negative inclination. B: Orthogonal vector plot of standard thermal demagnetization whole rock transitional series anorthosite. NRM intensity is 9.82 x 10^{-7} A m^2. Inset: equal area stereonet projection, labeled points are steps in °C. Filled circles, positive inclination; open circles, negative inclination.

Fig. DR6. Magnetic hysteresis and thermal demagnetization of felsic dike samples. A: Magnetic hysteresis data from felsic dike bulk sample (solid circles) and single feldspar crystals (open circles). Plot abbreviations as in Fig. 1. B: Orthogonal vector plot of standard thermal demagnetization of whole rock felsic dike. NRM intensity is 4.13 x 10^{-6} A m^2. C-E: Orthogonal vector plots of CO_2 laser thermal demagnetization of oriented feldspar from felsic dike. Boxes, inclination; circles, declination. Numbers points are ^{o}C. C: NRM intensity is 3.11 x 10^{-10} A m^2. D: NRM intensity is 2.19 x 10^{-10} A m^2. E: NRM intensity is 2.08 x 10^{-10} A m^2. F: Equal area stereonet of characteristic remanent directions from C-E. Open symbols represent negative inclinations, dashed circles show maximum angular deviation from principal component fits.

Fig. DR7. Scanning electron microscopy of SIIS anorthosite. A: Backscattered electron micrographs of whole rock showing millimeter size titanomagnetite grains with Fe-Ti-oxide exsolution. B: Ti-oxide enriched region with <100 μm Fe-rich exsolved needles, enlarged view from red box in (A). C: Enlarged view of Fe-rich oxide needles, from red box in (B).

Fig. DR8. Scanning electron microscopy of SIIS feldspar. A: Backscattered electron micrographs showing <20 μm length Fe-oxide needles in two directions. B: Fe-oxide needles with lengths <5 μm.

Fig. DR9. Virtual Geomagnetic Poles (VGPs) of Sept-Îles oriented feldspars. Open symbols: negative latitudes; closed symbols: positive latitudes. VGP's have been assigned A, B and C types (see Methods). Circles: Type A VGPs; squares: Type B VGPs; diamonds: Type C VGPs. Large symbols and shaded regions show mean VGPs and 95% confidence intervals, respectively. This assignment implies a VGP cutoff angle separating normal secular variation from transitional directions of 35° for the data set.

DATA REPOSITORY TABLES

Table DR1. Characteristic remanent directions from SIIS anorthosite single feldspar crystals.

Table DR2. Characteristic remanent directions from SIIS felsic dike single feldspar crystals.

Table DR3. Hysteresis properties from SIIS groundmass and single crystals presented in Fig. 1D.

Table DR4. Estimate of anisotropy of thermoremanent magnetization of single plagioclase crystals from Sept-Îles Layered Series anorthosites.

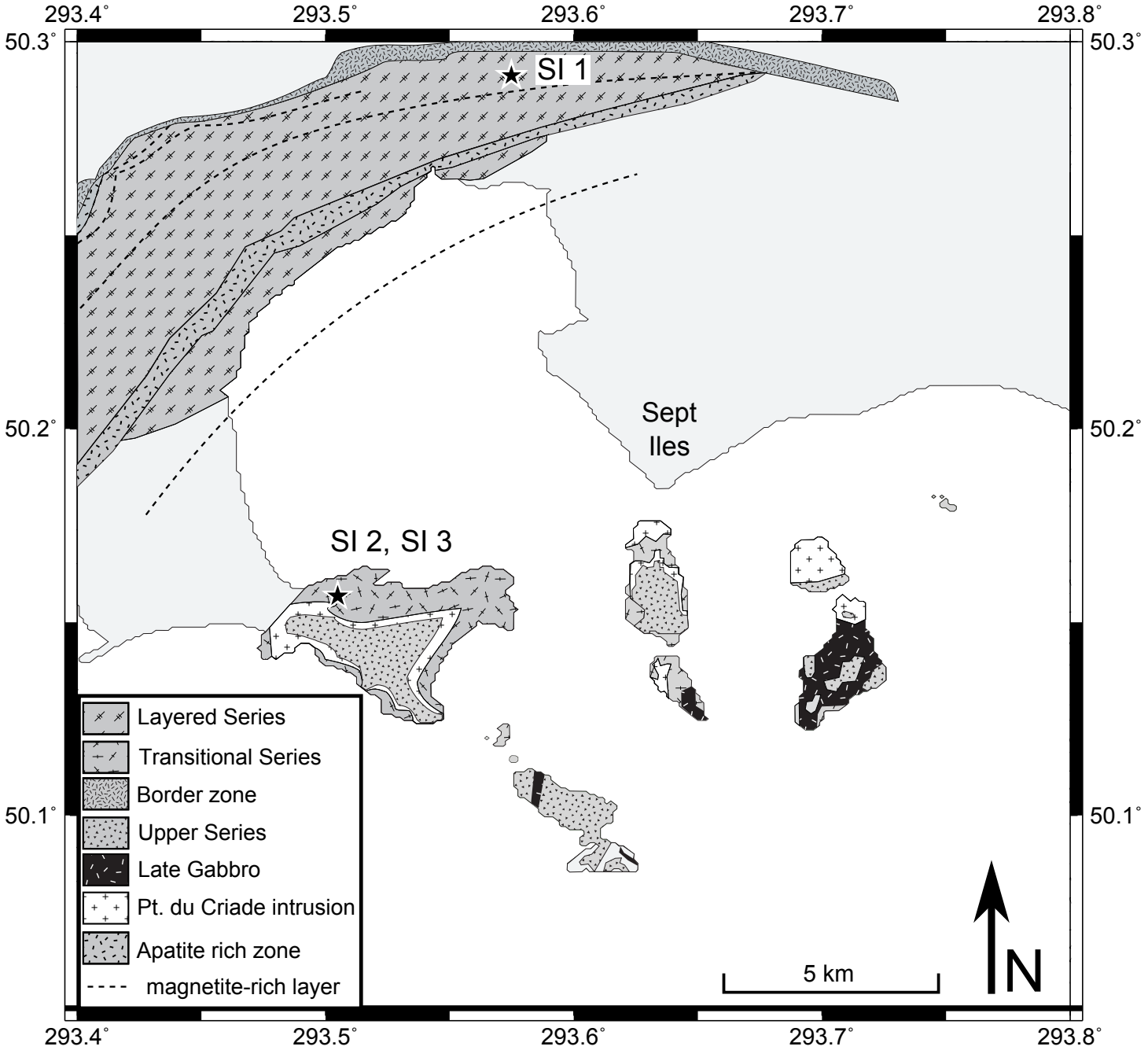
293.4˚
293.5˚
293.6˚
293.7˚
293.8˚
50.3˚
50.2˚
50.1˚
SI 1
Sept
Iles
SI 2, SI 3
Layered Series
Transitional Series
Border zone
Upper Series
Late Gabbro
Pt. du Criade intrusion
Apatite rich zone
magnetite-rich layer
5 km
N

Fig. DR1

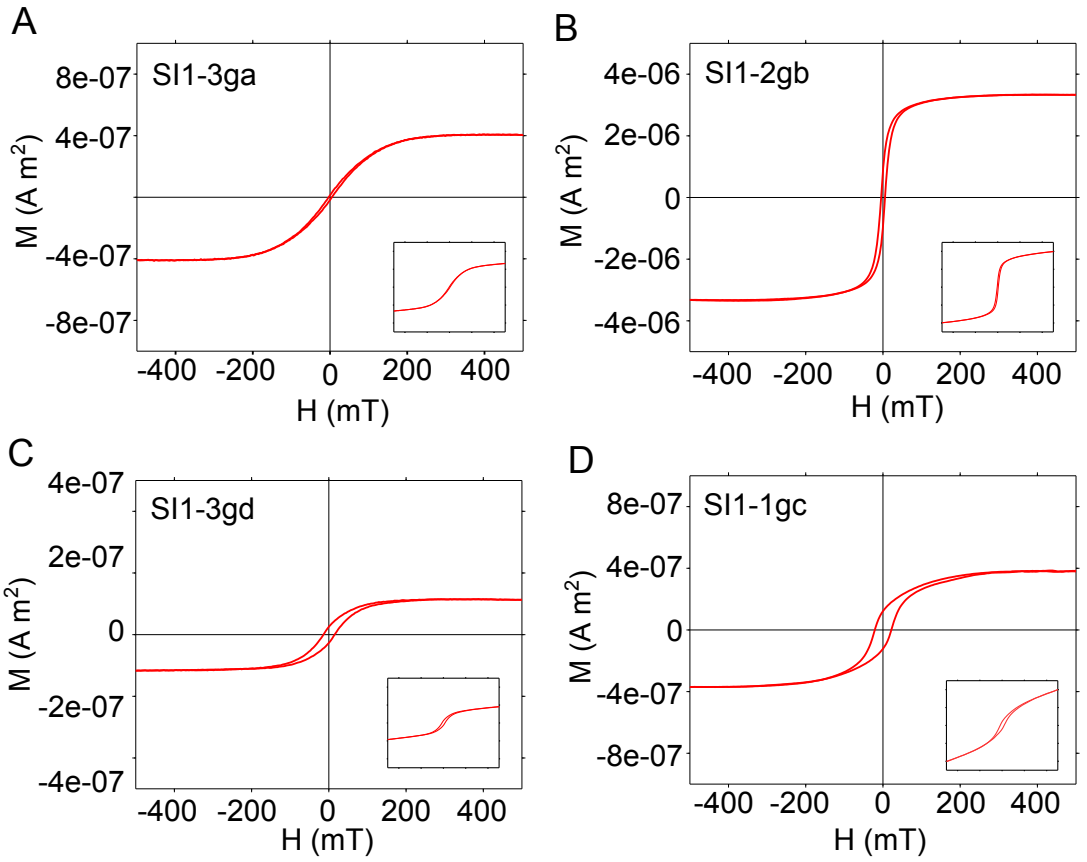
A
SI1-3ga
8e-07
4e-07
-4e-07
-8e-07
M (A m²)
-400 -200 0 200 400
H (mT)
B
SI1-2gb
4e-06
2e-06
0
-2e-06
-4e-06
M (A m²)
-400 -200 0 200 400
H (mT)
C
SI1-3gd
4e-07
2e-07
0
-2e-07
-4e-07
M (A m²)
-400 -200 0 200 400
H (mT)
D
SI1-1gc
8e-07
4e-07
0
-4e-07
-8e-07
M (A m²)
-400 -200 0 200 400
H (mT)

Fig. DR2

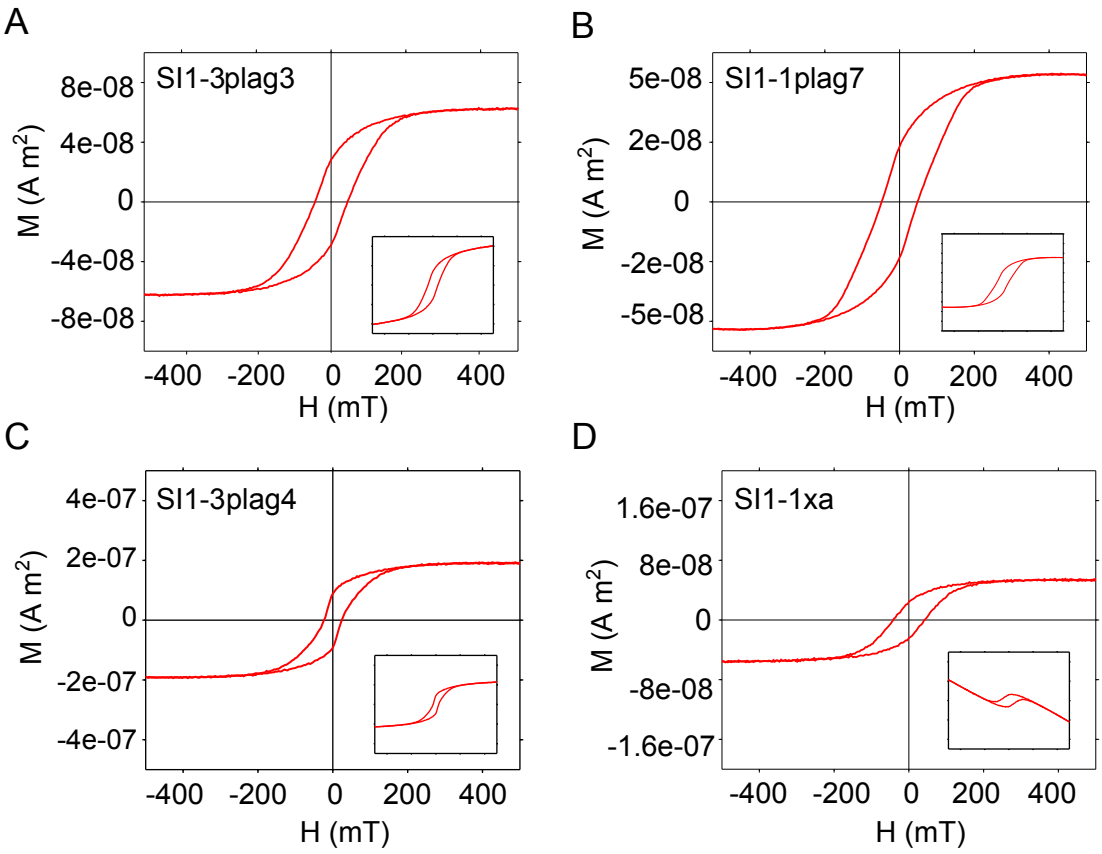
A
SI1-3plag3
8e-08
4e-08
0
-4e-08
-8e-08
M (A m2)
-400 -200 0 200 400
H (mT)
B
SI1-1plag7
5e-08
2e-08
0
-2e-08
-5e-08
M (A m2)
-400 -200 0 200 400
H (mT)
C
SI1-3plag4
4e-07
2e-07
0
-2e-07
-4e-07
M (A m2)
-400 -200 0 200 400
H (mT)
D
SI1-1xa
1.6e-07
8e-08
0
-8e-08
-1.6e-07
M (A m2)
-400 -200 0 200 400
H (mT)

Fig. DR3

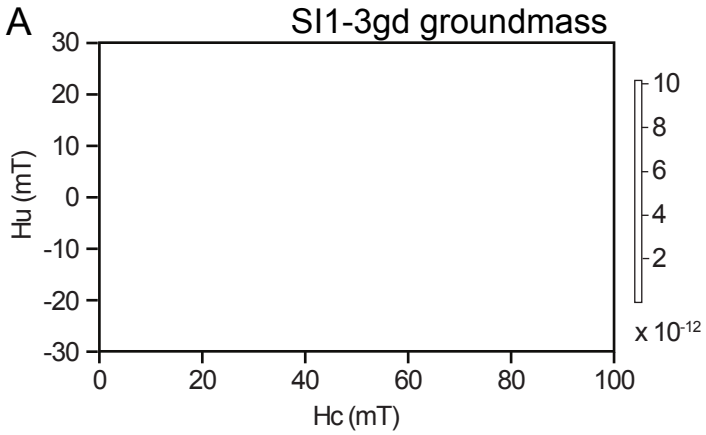

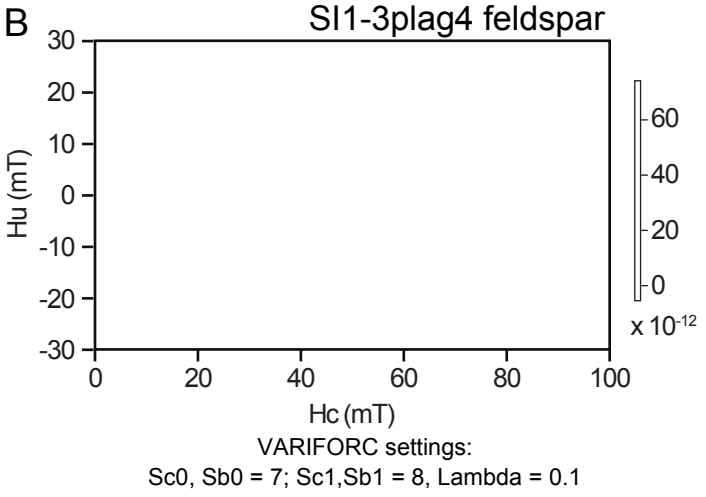

Processed using FORCinel 2.03 of Harrison & Feinberg (2008)

Fig. DR4

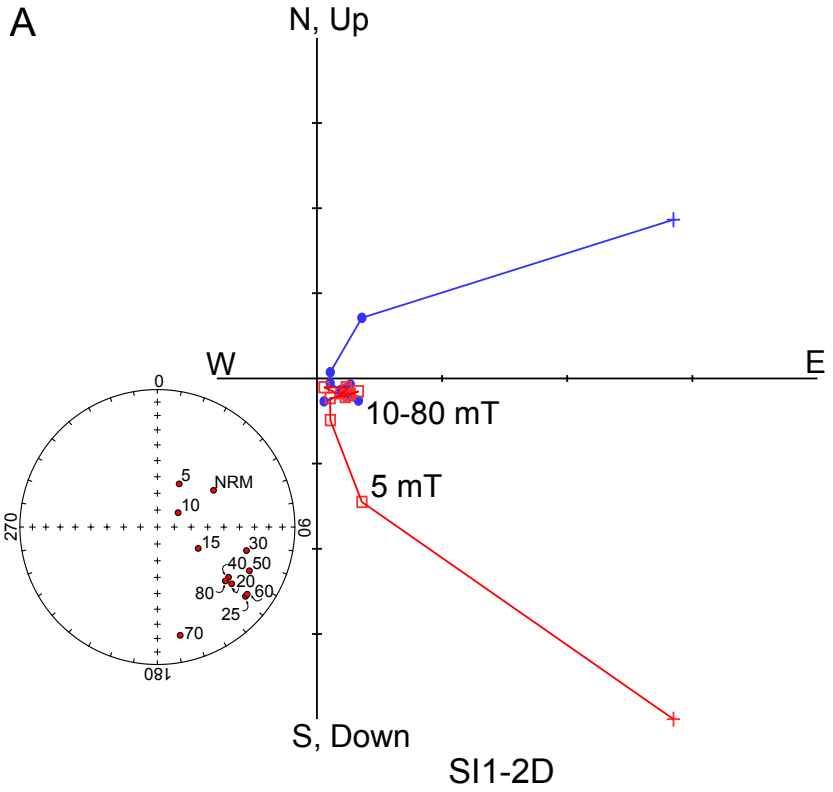
A
N, Up
W
E
S, Down
10-80 mT
5 mT
0
90
180
270
5
NRM
10
15
30
40
50
20
60
80
25
70
SI1-2D

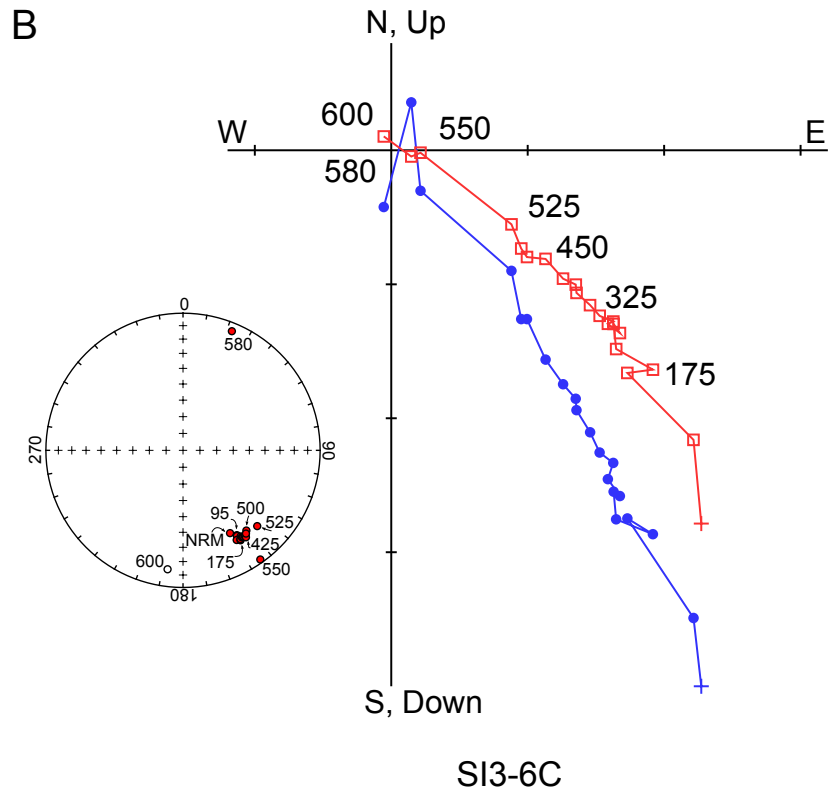
B
N, Up
W
E
S, Down
600
550
580
525
450
325
175
0
90
180
270
580
95
500
525
NRM
425
600
175
550
SI3-6C

Fig. DR5

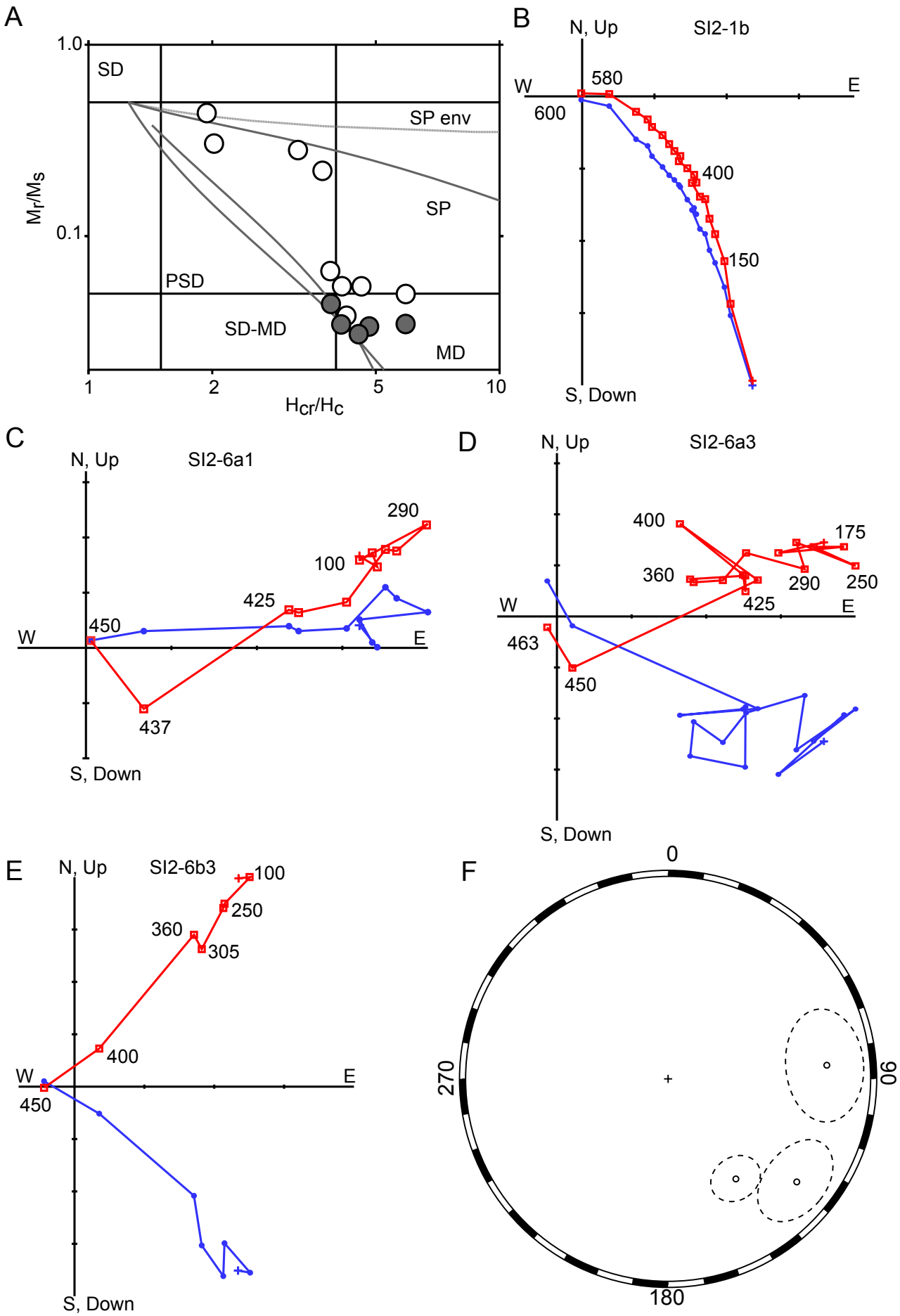
A
1.0
SD
SP env
SP
0.1
PSD
SD-MD
MD
1
2
5
10
M_r/M_s
H_{cr}/H_c
B
N, Up
SI2-1b
W
E
580
600
400
150
S, Down
C
N, Up
SI2-6a1
290
100
425
450
W
E
437
S, Down
D
N, Up
SI2-6a3
400
175
360
290
250
425
W
E
463
450
S, Down
E
N, Up
SI2-6b3
100
250
360
305
400
W
E
450
S, Down
F
0
270
90
180

Fig. DR6

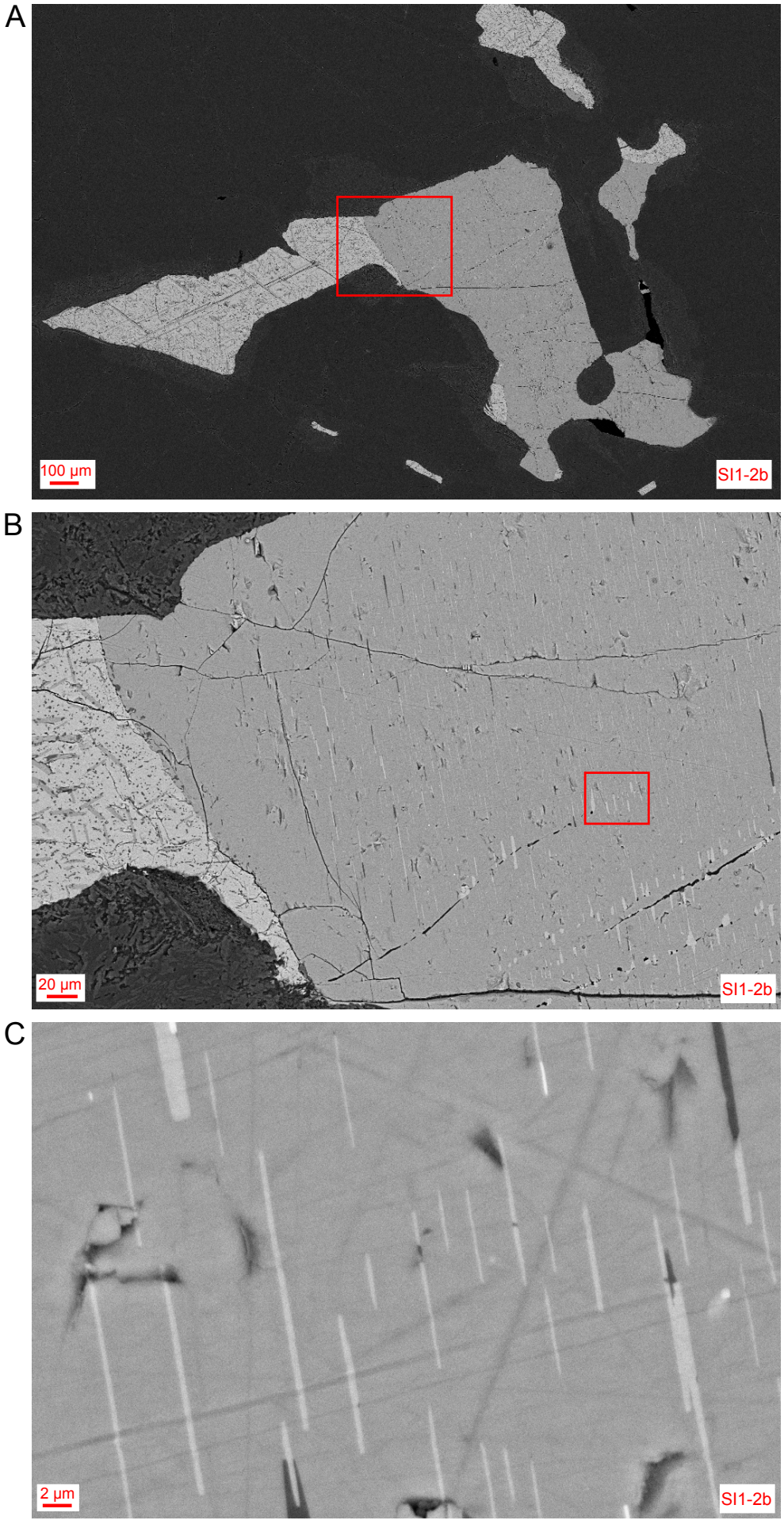

Fig. DR7

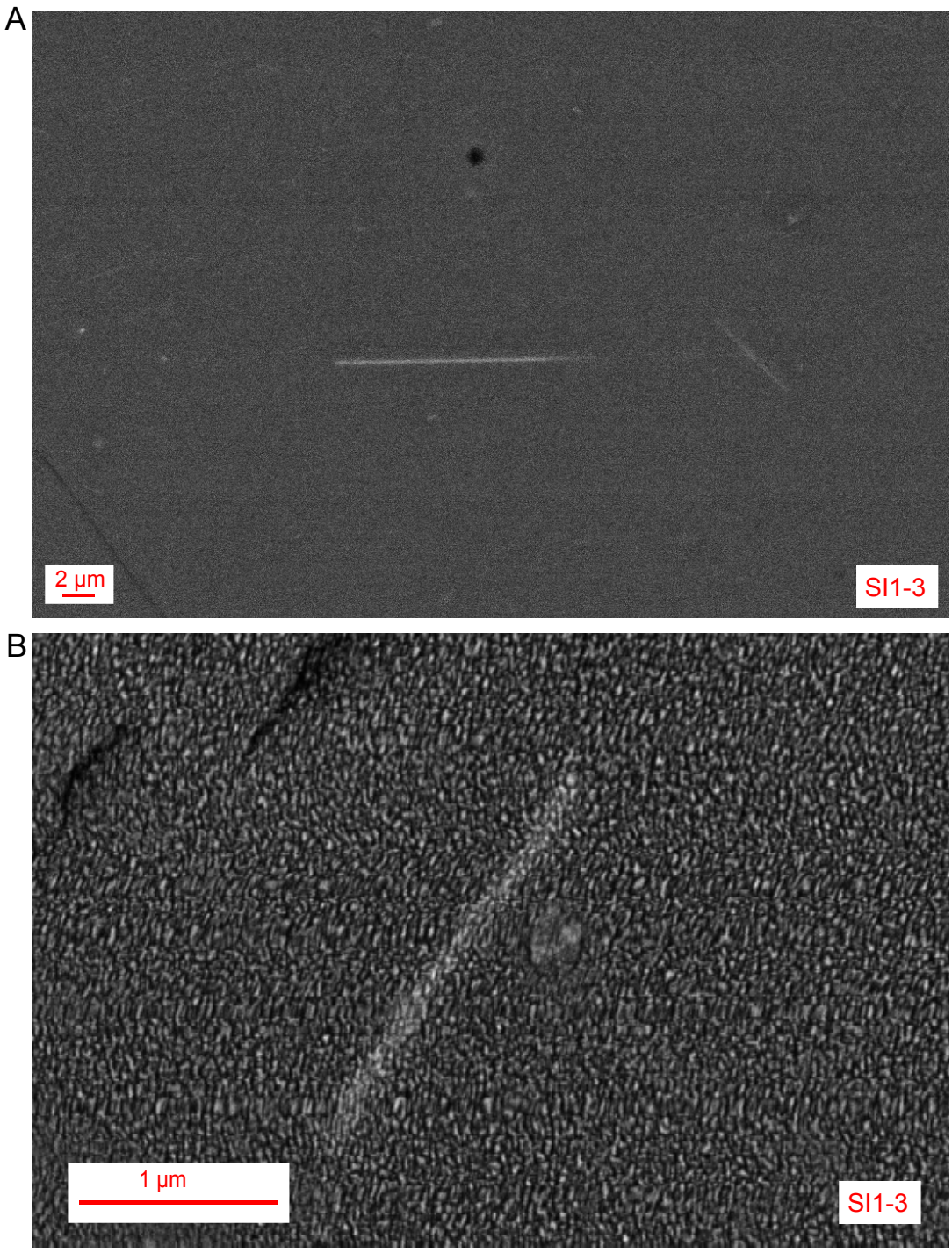

Fig. DR8

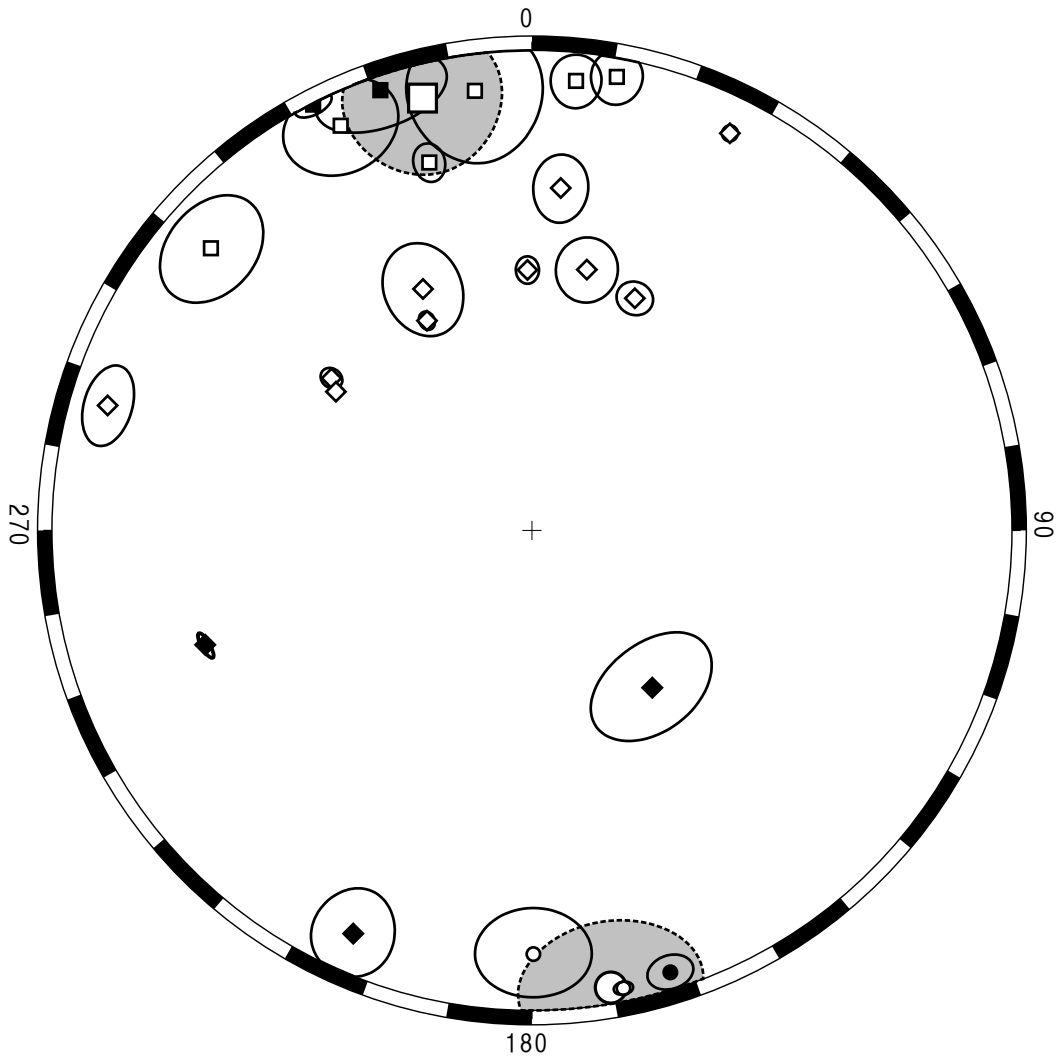

Fig. DR9

DATA REPOSITORY TABLES

TABLE DR1: CHARACTERISTIC REMANENT DIRECTIONS FROM SIIS ANORTHOSITE SINGLE FELDSPAR CRYSTALS

Sample	Temperature (°C)	N	Dec (°)	Inc (°)	MAD (°)
Type A					
si1-2a4	425 - 520*	6	280.2	-42.9	10.0
si1-2b1a†	360 - 400*	4	296.3	-41.6	1.6
si1-2b1b†	400 - 475	4	306.0	-38.0	4.2
Type B					
si1-1c1	450 - 500	3	135.2	39.1	10.7
si1-1c5	475 - 580*	5	123.2	47.4	10.0
si1-2a2	425 - 475	3	119.8	23.3	15.4
si1-2a3	400 - 450	3	160.7	44.1	10.0
si1-2b5	450 - 520	4	102.8	9.6	6.3
si1-2b6	425 - 475	3	108.1	12.2	6.1
si1-2b10	400 - 580*	4	133.6	10.5	4.2
si1-2b14	400 - 437	3	133.1	49.0	2.8
Type C					
si1-2a1	360 - 500*	4	154.5	-29.2	2.0
si1-2a5	400 - 450	3	343.4	34.8	16.7
si1-2b2a†	425 - 475	3	188.2	49.9	6.0
si1-2b2b†	400 - 450	3	252.6	68.2	1.3
si1-2b3	400 - 500	5	275.5	14.1	10.2
si1-2b4	375 - 500*	7	93.2	-16.3	1.8
si1-2b8	400 - 580*	6	136.5	-37.3	2.6
si1-2b15	375 - 413*	4	170.6	-15.0	2.8
si1-3a1	425 - 520	5	150.6	-21.9	10.7
si1-3a2	425 - 475	3	172.2	-18.6	0.6
si1-3a5	360 - 400*	4	122.6	-21.9	7.2
si1-3c6	400 - 450*	4	128.2	-44.5	6.0
si1-3c7	400 - 450	3	123.5	-53.4	3.0

N: number of temperature steps, Dec: declination, Inc: inclination, MAD: maximum angular deviation
*Origin included for principal component analysis.
†Samples appended with “a” or “b” were sub-sampled from the same feldspar crystal.
Sample nomenclature: SI(Site #)-(hand sample #)(core letter)(oriented crystal #)
e.g., si1-2a4: SI(Site 1)-(hand sample 2)(core A)(oriented crystal 4)

TABLE DR2: CHARACTERISTIC REMANENT DIRECTIONS FROM SIIS FELSIC DIKE SINGLE FELDSPAR CRYSTALS

Sample	Temperature (°C)	N	Dec (°)	Inc (°)	MAD (°)
si2-6a1	400 - 450*	6	85.1	-22.5	18.9
si2-6a3	425 - 463	3	128.7	-19.8	15.2
si2-6b3	305 - 400*	4	145.9	-40.2	9.5

N: number of temperature steps, Dec: declination, Inc: inclination, MAD: maximum angular deviation

* Origin included for principal component analysis.

TABLE DR3: HYSTERESIS PROPERTIES FROM SIIS GROUNDMASS AND SINGLE CRYSTALS PRESENTED IN FIG. 1D

Sample	Unit	Type	Mr (nAm^2)	Ms (nAm^2)	Hc (mT)	Hcr (mT)
si1-1ga	Layered Series	groundmass	10.43	115.4	4.959	11.41
si1-1gb	Layered Series	groundmass	97.77	549.0	7.796	15.95
si1-1gc	Layered Series	groundmass	122.1	374.8	21.41	29.14
si1-1gd	Layered Series	groundmass	20.88	50.34	44.93	81.16
si1-2ga	Layered Series	groundmass	16.73	364.0	5.498	22.89
si1-2gb	Layered Series	groundmass	639.7	3244	4.903	6.902
si1-2gc	Layered Series	groundmass	3.931	51.07	4.953	14.98
si1-3ga	Layered Series	groundmass	7.898	203.5	4.229	27.24
si1-3gd	Layered Series	groundmass	26.22	114.8	14.47	33.36
si1-1xa	Layered Series	crystal	2.422	5.434	41.95	65.77
si1-1plag4	Layered Series	crystal	65.09	206.7	24.78	54.53
si1-1plag6	Layered Series	crystal	10.91	26.62	43.73	68.67
si1-1plag7	Layered Series	crystal	22.28	51.09	48.02	92.01
si1-3plag3	Layered Series	crystal	28.70	61.76	43.29	79.85
si1-3plag4	Layered Series	crystal	90.48	190.5	23.74	38.91
si3-2plag1	Transitional Series	crystal	14.31	45.13	21.94	32.45
si3-2plag2	Transitional Series	crystal	4.324	20.79	21.97	53.97
si3-2plag6	Transitional Series	crystal	157.4	836.1	22.76	51.82

TABLE DR4: ESTIMATE OF ANISOTROPY OF THERMOREMANENT MAGNETIZATION OF SINGLE PLAGIOCLASE CRYSTALS FROM SEPT-ÎLES LAYERED SERIES ANORTHOSITES

	Applied field	Total TRM		
Sample	(Dec, Inc)	Dec (°)	Inc (°)	Δ(°)
si1-1x14	(0, -90)	224.5	-67.2	22.8
si1-2x5	(0, -90)	222.8	-70.8	19.2
si1-2x11	(0, +90)	100.2	72.4	17.6
si1-2x13	(0, -90)	351.9	-64.2	25.8
si1-3x32	(0, +90)	142.2	75.7	14.3

Average Δ (+/- s.d.): 19.9 +/- 4.0